

# Inferring Changes in Summertime Surface Ozone–NO<sub>x</sub>–VOC Chemistry over U.S. Urban Areas from Two Decades of Satellite and Ground-Based Observations

Xiaomeng Jin,\* Arlene Fiore, K. Folkert Boersma, Isabelle De Smedt, and Lukas Valin



Cite This: *Environ. Sci. Technol.* 2020, 54, 6518–6529



Read Online

ACCESS |



Metrics & More

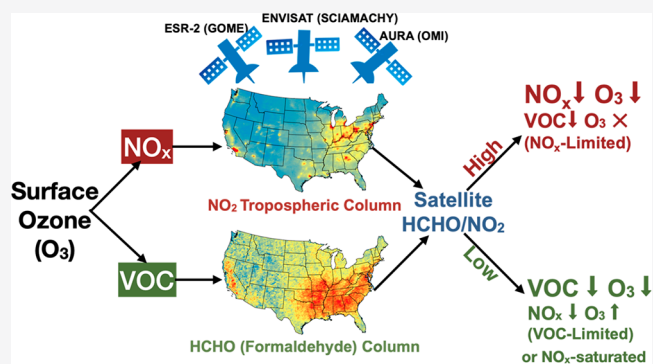


Article Recommendations



Supporting Information

**ABSTRACT:** Urban ozone (O<sub>3</sub>) formation can be limited by NO<sub>x</sub>, VOCs, or both, complicating the design of effective O<sub>3</sub> abatement plans. A satellite-retrieved ratio of formaldehyde to NO<sub>2</sub> (HCHO/NO<sub>2</sub>), developed from theory and modeling, has previously been used to indicate O<sub>3</sub> formation chemistry. Here, we connect this space-based indicator to spatiotemporal variations in O<sub>3</sub> recorded by on-the-ground monitors over major U.S. cities. High-O<sub>3</sub> events vary nonlinearly with OMI HCHO and NO<sub>2</sub>, and the transition from VOC-limited to NO<sub>x</sub>-limited O<sub>3</sub> formation regimes occurs at higher HCHO/NO<sub>2</sub> value (3 to 4) than previously determined from models, with slight intercity variations. To extend satellite records back to 1996, we develop an approach to harmonize observations from GOME and SCIAMACHY that accounts for differences in spatial resolution and overpass time. Two-decade (1996–2016) multisatellite HCHO/NO<sub>2</sub> captures the timing and location of the transition from VOC-limited to NO<sub>x</sub>-limited O<sub>3</sub> production regimes in major U.S. cities, which aligns with the observed long-term changes in urban–rural gradient of O<sub>3</sub> and the reversal of O<sub>3</sub> weekend effect. Our findings suggest promise for applying space-based HCHO/NO<sub>2</sub> to interpret local O<sub>3</sub> chemistry, particularly with the new-generation satellite instruments that offer finer spatial and temporal resolution.



## INTRODUCTION

Human exposure to ground-level ozone (O<sub>3</sub>) is associated with increased risk of cardiovascular and respiratory diseases, and has been linked to 250 000 O<sub>3</sub>-related premature deaths in 2015 globally,<sup>1</sup> and 11 700 deaths over the United States (U.S.).<sup>2</sup> In the troposphere, O<sub>3</sub> is produced from photochemical reactions involving its precursors: nitrogen oxides (NO<sub>x</sub>: NO + NO<sub>2</sub>) and volatile organic compounds (VOCs). It is well established that O<sub>3</sub> formation throughout much of the troposphere is largely controlled by the availability of NO<sub>x</sub> (NO<sub>x</sub>-limited), but in regions with high NO<sub>x</sub> emissions, such as metropolitan areas, O<sub>3</sub> formation can be VOC-limited or in transition between these regimes.<sup>3,4</sup> Identifying the most effective emissions control strategy to lower the O<sub>3</sub> exposure of a densely populated metropolitan area requires knowledge of the local O<sub>3</sub> formation chemistry.

While current satellite-based spectrometers do not retrieve ground-level O<sub>3</sub> abundances, they have provided continuous global observations for two species indicative of O<sub>3</sub> precursors, namely nitrogen dioxide (NO<sub>2</sub>) for NO<sub>x</sub><sup>5–7</sup> and formaldehyde (HCHO) for VOC,<sup>8–13</sup> for over two decades. In theory, the ratio of HCHO to NO<sub>2</sub> (HCHO/NO<sub>2</sub>) reflects the relative availability of NO<sub>x</sub> and total organic reactivity to hydroxyl radicals.<sup>14,15</sup> We build here upon earlier work proposing this

satellite-based HCHO/NO<sub>2</sub> as an indicator of O<sub>3</sub> sensitivity to its NO<sub>x</sub> versus VOC precursors.<sup>16–19</sup> All of these prior studies use theory as represented in models to link column-based HCHO/NO<sub>2</sub> with surface O<sub>3</sub> sensitivity.<sup>16–19</sup> Models, however, can be biased,<sup>20</sup> and airborne measurements suggest large uncertainty in the HCHO/NO<sub>2</sub> threshold values between O<sub>3</sub> production regimes.<sup>21</sup> Also, modeled and satellite retrieved HCHO and NO<sub>2</sub> often disagree,<sup>19,22,23</sup> and the difference varies by satellite retrievals.<sup>19,24</sup> To overcome these limitations, we derive the threshold values marking transitions in O<sub>3</sub> formation regimes entirely from observations by directly connecting space-based HCHO/NO<sub>2</sub> with ground-based measurements of O<sub>3</sub>.

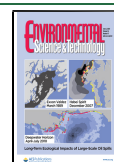
Over the U.S., nationwide anthropogenic NO<sub>x</sub> emissions are estimated to have declined by 31% from 1997 to 2016.<sup>25</sup> Correspondingly, satellite-retrieved NO<sub>2</sub> tropospheric columns are declining,<sup>7,26,27</sup> although relating NO<sub>2</sub> columns directly to

Received: December 20, 2019

Revised: April 28, 2020

Accepted: April 29, 2020

Published: April 29, 2020



NO<sub>x</sub> emissions requires accounting for lifetime changes,<sup>28</sup> and accurate partitioning between anthropogenic versus background sources of NO<sub>2</sub>.<sup>22,29</sup> Despite the widespread decrease of NO<sub>x</sub> emissions, observed O<sub>3</sub> trends are heterogeneous in space and time: decreasing in summer over less urbanized areas, and increasing in winter, night, and urban cores, due to the nonlinear relationship between O<sub>3</sub> production and NO<sub>x</sub>.<sup>30–33</sup> As NO<sub>x</sub> emissions continue to decline, O<sub>3</sub> formation over VOC-limited urban areas is transitioning toward the NO<sub>x</sub>-limited regime,<sup>19,34–36</sup> but the observed long-term O<sub>3</sub> trends may also reflect changes in VOC reactivity,<sup>37</sup> as well as meteorology.<sup>38</sup> U.S. anthropogenic VOC emissions from vehicles and industry are estimated to have declined by 22% from 1997 to 2016,<sup>25</sup> while volatile chemical product emissions may be growing.<sup>39</sup> Regionally, summertime U.S. VOC emissions are dominated by biogenic sources, particularly highly reactive isoprene, that vary with meteorology and vegetation density.<sup>40</sup>

A key policy-relevant metric is the turning point between VOC-limited and NO<sub>x</sub>-limited O<sub>3</sub> formation regimes. It remains uncertain as to which (and whether) U.S. cities have reached this turning point, and how closely long-term changes in O<sub>3</sub> follow transitions in O<sub>3</sub> production regimes, particularly in light of the strong sensitivity of O<sub>3</sub> to meteorological variability.<sup>41,42</sup> Previous studies used observations of HCHO/NO<sub>2</sub> from single satellite instrument, such as Ozone Monitoring Instrument (OMI), which dates back to 2005.<sup>17–19</sup> The newly developed, consistently retrieved multisatellite HCHO and NO<sub>2</sub> products, available from the EU FP7-project Quality Assurance for Essential Climate Variables (QA4ECV),<sup>43–49</sup> offer a new opportunity to extend the record back by a decade to 1996. We first assess if space-based HCHO/NO<sub>2</sub> captures the nonlinearity of O<sub>3</sub> chemistry by matching daily OMI observation with ground-based O<sub>3</sub> measurements over polluted areas. We find a robust relationship between space-based HCHO/NO<sub>2</sub> and the O<sub>3</sub> response patterns that is qualitatively similar but quantitatively distinct across cities. Next, we link the long-term changes in the harmonized multisatellite HCHO/NO<sub>2</sub> to changes in urban–rural O<sub>3</sub> gradients and the O<sub>3</sub> weekend effect from 1996 to 2016. We show that this multisatellite HCHO/NO<sub>2</sub> complements ground-based networks by providing insights into spatial heterogeneity and long-term evolution of O<sub>3</sub> formation regimes, which could be valuable for future applications over regions lacking dense ground-based monitors.

## MATERIALS AND METHODS

**Multisatellite Observations of O<sub>3</sub> Precursors.** We use 21-year (1996–2016) multisatellite products of tropospheric NO<sub>2</sub> (Ω<sub>NO<sub>2</sub></sub>) and HCHO (Ω<sub>HCHO</sub>) vertical columns developed under the QA4ECV project that retrieves products consistently from three satellite instruments: Global Ozone Monitoring Experiment (GOME), Scanning Imaging Absorption spectrometer for Atmospheric CHartography (SCIAMACHY) and OMI.<sup>43–49</sup> The nadir resolution is 24 × 13 km<sup>2</sup> for OMI, 60 × 30 km<sup>2</sup> for SCIAMACHY and 320 × 40 km<sup>2</sup> for GOME. The overpass time is around 1:30 PM local time for OMI, 10:00 AM for SCIAMACHY, and 10:30 AM for GOME. The a priori vertical profiles used for QA4ECV products are obtained from the same chemical transport model (TMS-MP),<sup>50</sup> which are better suited for analyzing space-based HCHO/NO<sub>2</sub> than products developed with different prior profiles. The retrieval algorithms are briefly described in the Supporting Information

(SI, S1). We select daily Level-2 observations with (1) no processing error; (2) less than 10% snow or ice coverage; (3) solar zenith angle less than 80° for NO<sub>2</sub>, and 70° for HCHO; (4) cloud radiance fractions <0.5. For OMI, we exclude the first and last five rows, which contain large pixels retrieved on the swath edges, and select the rows 5 to 23, which are unaffected by row anomalies throughout the study period.<sup>51</sup> We grid Level-2 swaths by calculating area weighted averages (S2).

**Seasonal Harmonization of GOME, SCIAMACHY, and OMI.** To study the long-term changes in HCHO, NO<sub>2</sub>, and HCHO/NO<sub>2</sub>, we construct seasonal average Ω<sub>HCHO</sub> and Ω<sub>NO<sub>2</sub></sub> from the three satellites by calculating the area-weighted averages from 1996 to 2016. The long-term satellite records are based on OMI observations for the years after 2005, the harmonized SCIAMACHY observations for 2002–2004, and harmonized GOME observations before 2002. Even with the consistent algorithms for retrieving NO<sub>2</sub> and HCHO under the QA4ECV project, multisatellite retrievals still need to be harmonized to account for differences in horizontal resolution, overpass time, and any instrumental offsets. We adjust SCIAMACHY and GOME HCHO and NO<sub>2</sub> data with reference to OMI, because OMI has the finest spatial resolution, and the satellites are best able to capture chemical conditions controlling O<sub>3</sub> production during the OMI afternoon overpass, when mixing depths and O<sub>3</sub> production rates are closest to their daily maxima. We first adjust SCIAMACHY Ω<sub>NO<sub>2</sub></sub> by decomposing the instrumental differences between SCIAMACHY and OMI into two factors: (1) those associated with different overpass timing or instrumental offsets, which we estimate as the difference in OMI Ω<sub>NO<sub>2</sub></sub> and SCIAMACHY Ω<sub>NO<sub>2</sub></sub> during the overlap period (2005–2011) at a coarse resolution at which we assume the difference is independent of the instrumental resolution ( $\overline{\Delta\Omega_{\text{NO}_2\text{-Coarse}}}$ , Figure S1); (2) those caused by resolution (RC<sub>NO<sub>2</sub></sub>, Figure S2), which we estimate as the relative change in OMI Ω<sub>NO<sub>2</sub></sub> at a fine-resolution (0.125° × 0.125°) versus a coarse-resolution (2° × 0.5°) grid that is close to the nadir resolution of GOME (RC<sub>NO<sub>2</sub>, OMI</sub>, S3). While previous studies assumed constant resolution correction factors,<sup>27,52</sup> we find that RC<sub>NO<sub>2</sub></sub> varies with time, especially over urban areas, and the spatial gradients in Ω<sub>NO<sub>2</sub></sub> are larger when Ω<sub>NO<sub>2</sub></sub> is higher earlier in the record (Figure S3). Assuming a time-invariant RC<sub>NO<sub>2</sub></sub> may thus underestimate the steepness of spatial gradients at high Ω<sub>NO<sub>2</sub></sub>. We apply the relative temporal variability estimated from RC<sub>NO<sub>2</sub>, SCIA</sub> to the long-term summertime average RC<sub>NO<sub>2</sub>, OMI</sub> ( $\overline{\text{RC}_{\text{NO}_2, \text{OMI}}}$ ). RC<sub>NO<sub>2</sub>, OMI</sub> and RC<sub>NO<sub>2</sub>, SCIA</sub> correlate well in time (Figure S4), though their absolute values differ. Combining these factors, the adjusted SCIAMACHY Ω<sub>NO<sub>2</sub></sub> (Ω<sub>NO<sub>2</sub>, adj</sub>) at year *yr* season *m* (we focus on summer, June–July–August) and grid cell *x* is estimated as follows:

$$\Omega_{\text{NO}_2, \text{adj}}(x_f, yr, m) = (\Omega_{\text{NO}_2, \text{coarse}}(x_c, yr, m) + \overline{\Delta\Omega_{\text{NO}_2, \text{Coarse}}}(x_c, m)) \times \overline{\text{RC}_{\text{NO}_2}}(x_f, x_c, yr, m) \quad (1)$$

where  $\overline{\Delta\Omega_{\text{NO}_2, \text{Coarse}}}(x_c, m)$  is the difference between OMI Ω<sub>NO<sub>2</sub></sub> and SCIAMACHY Ω<sub>NO<sub>2</sub></sub> at coarse resolution averaged during the overlap period (*n* years):

$$\overline{\Delta\Omega_{\text{NO}_2, \text{Coarse}}}(x_c, m) = \frac{1}{n} \sum_{yr=2005}^{yr=2011} (\Omega_{\text{NO}_2, \text{OMI, coarse}}(x_c, yr, m) - \Omega_{\text{NO}_2, \text{SCIA, coarse}}(x_c, yr, m)) \quad (2)$$

where  $RC_{NO_2}(x_f, x_c, yr, m)$  is the resolution correction factor,  $x_f$  is the grid cell at fine resolution, and  $x_c$  is the coarse grid cell where  $x_f$  falls.

$$RC_{NO_2}(x_f, x_c, yr, m) = \overline{RC_{NO_2\_OMI}(x_f, x_c, m)} \times \frac{RC_{NO_2\_SCIA}(x_f, x_c, yr, m)}{RC_{NO_2\_SCIA}(x_f, x_c, m)} \quad (3)$$

$$\overline{RC_{NO_2\_OMI}(x_f, x_c, m)} = \frac{1}{n} \sum_{yr=2005}^{yr=2016} \frac{\Omega_{NO_2\_OMI\_fine}(x_f, yr, m)}{\Omega_{NO_2\_OMI\_coarse}(x_c, yr, m)} \quad (4)$$

$$RC_{NO_2\_SCIA}(x_f, x_c, yr, m) = \frac{\Omega_{NO_2\_SCIA\_fine}(x_f, yr, m)}{\Omega_{NO_2\_SCIA\_coarse}(x_c, yr, m)} \quad (5)$$

$$\overline{RC_{NO_2\_SCIA}(x_f, x_c, m)} = \frac{1}{n} \sum_{yr=2002}^{yr=2012} RC_{NO_2\_SCIA}(x_f, x_c, yr, m) \quad (6)$$

To harmonize GOME  $\Omega_{NO_2}$ , we apply the same correction factors that we applied to SCIAMACHY except that the temporal variability in  $RC_{NO_2}$  is driven by the variability in  $RC_{NO_2}$  of GOME. We do not adjust for any systematic differences between GOME and SCIAMACHY at coarse resolution, because the overpass time is close, and the overlap period (August 2002 to June 2003) does not cover an entire summer.

We similarly decompose the instrumental differences in  $\Omega_{HCHO}$  to differences caused by resolution ( $RC_{HCHO\_OMI}$ ) versus overpass time ( $\Delta\Omega_{HCHO\_Coarse}$ ). We find that  $RC_{HCHO\_OMI}$  is much smaller than  $\Delta\Omega_{HCHO\_Coarse}$  and the spatial pattern of  $RC_{HCHO\_OMI}$  tends to be noisy (Figure S5). We find little resolution dependence of the difference between OMI  $\Omega_{HCHO}$  and SCIAMACHY  $\Omega_{HCHO}$ , likely due to widespread summertime isoprene emissions, the dominant summertime precursor to HCHO over the U.S., as well as HCHO produced during oxidation of longer-lived VOCs.<sup>51</sup> Therefore, we do not apply a resolution correction to SCIAMACHY  $\Omega_{HCHO}$  or GOME  $\Omega_{HCHO}$ . We calculate the climatology of the systematic difference ( $\overline{\Delta\Omega_{HCHO}}$ ) between OMI  $\Omega_{HCHO}$  and SCIAMACHY  $\Omega_{HCHO}$  at  $0.25^\circ \times 0.25^\circ$  resolution, and adjust  $\Omega_{HCHO}$  ( $\Omega_{HCHO\_adj}$ ) by applying these differences to the original SCIAMACHY and GOME  $\Omega_{HCHO}$  ( $\Omega_{HCHO\_Ori}$ ) for the years without OMI observations:

$$\Omega_{HCHO\_adj}(x, yr, m) = \Omega_{HCHO\_Ori}(x, yr, m) + \overline{\Delta\Omega_{HCHO}}(x, m) \quad (7)$$

$$\overline{\Delta\Omega_{HCHO}}(x, m) = \frac{1}{n} \sum_{yr=2005}^{yr=2011} (\Omega_{HCHO\_OMI}(x, yr, m) - \Omega_{HCHO\_SCIA}(x, yr, m)) \quad (8)$$

The systematic difference is mainly attributed to the diel cycle in HCHO.<sup>54</sup> As we adjust the morning retrieval of HCHO with respect to the afternoon retrieval, upward adjustment is expected due to the diel cycle in temperature, which controls biogenic VOC emissions, and in OH, which controls HCHO production from its parent VOCs (Figure S5).<sup>40,55</sup>

**Connecting Satellite HCHO/NO<sub>2</sub> with Ground-Based O<sub>3</sub> Observations.** We use observations of hourly O<sub>3</sub> from the U.S. Air Quality System (AQS) from 1996 to 2016. We first aggregate daily OMI data (used in Figure 1) by sampling the

gridded daily OMI  $\Omega_{HCHO}$  and  $\Omega_{NO_2}$  ( $0.125^\circ \times 0.125^\circ$ ) coincident with ground-based observations of O<sub>3</sub>. Retrievals from SCIAMACHY and GOME are not used for daily analysis because harmonization at the daily time scale is unrealistic. We average hourly O<sub>3</sub> measurements at 1 PM and 2 PM local time to match the OMI overpass time. We first select 1221 O<sub>3</sub> monitors located in polluted regions, defined as summertime 2005–2016 average OMI  $\Omega_{NO_2} > 1.5 \times 10^{15}$  molecules/cm<sup>2</sup>. OMI retrieved  $\Omega_{NO_2}$  and  $\Omega_{HCHO}$  are sampled daily over AQS O<sub>3</sub> sites for the warm season (May to October) from 2005 to 2016, yielding over 700 000 paired observations, and we calculate the probability of O<sub>3</sub> exceeding 70 ppb from this data set. Next, we focus on seven metropolitan areas to evaluate the satellite-based HCHO/NO<sub>2</sub> and study the long-term evolution of O<sub>3</sub> production regimes from 1996 to 2016, as the resolution of the harmonized satellite products ( $\sim 10$  km) is more suitable for studying cities spanning larger areas. We first select Los Angeles, New York, and Chicago, the three most populous cities in the U.S.A. We then include four additional cities: Washington, DC. Pittsburgh, Atlanta, and Houston, where long-term ground-based observations of O<sub>3</sub> and NO<sub>x</sub> are available, and which also cover different U.S. climate regions. To assess if satellite HCHO/NO<sub>2</sub> captures the long-term changes in O<sub>3</sub> production regimes, we include ground-based measurements of O<sub>3</sub> from 1996 to 2016 in each of the seven cities and their surrounding rural areas, from which we analyze the changes in urban–rural O<sub>3</sub> gradients, and the weekday-to-weekend differences defined as weekend (Saturday–Sunday) O<sub>3</sub> – weekday (Tuesday–Friday) O<sub>3</sub>.

## RESULTS AND DISCUSSION

**Nonlinear O<sub>3</sub> Chemistry Captured by Satellite-Based HCHO/NO<sub>2</sub>.** We first evaluate if satellite-based HCHO/NO<sub>2</sub> can capture the well-established nonlinearities in O<sub>3</sub> chemistry. Pusede et al.<sup>56</sup> proposed a conceptual framework that uses the observed O<sub>3</sub> exceedance probability to interpret the nonlinear dependence of O<sub>3</sub> production on precursor emissions. This framework assumes stagnant meteorology so that measured O<sub>3</sub> is sensitive to its local chemical production, and the local changes in chemical or depositional loss are insignificant on average. We follow this approach by calculating the probability that surface O<sub>3</sub> exceeds 70 ppbv (high-O<sub>3</sub> probability) at OMI overpass, given the OMI  $\Omega_{NO_2}$  and  $\Omega_{HCHO}$  (Figure 1a). Figure 1a, derived solely from observations, resembles O<sub>3</sub> isopleths that are typically generated with analytical models.<sup>4,57</sup> Consistent with O<sub>3</sub> isopleths, three regimes can be roughly identified from Figure 1a: (1) high  $\Omega_{NO_2}$  and low  $\Omega_{HCHO}$ , where high O<sub>3</sub> events become more likely at lower NO<sub>x</sub>, indicating NO<sub>x</sub>-saturated (or VOC-limited) chemistry; (2) low  $\Omega_{NO_2}$  and relatively high  $\Omega_{HCHO}$ , where the probability of high O<sub>3</sub> events increases with  $\Omega_{NO_2}$ , indicating NO<sub>x</sub>-limited chemistry; and (3) high  $\Omega_{NO_2}$  and high  $\Omega_{HCHO}$ , where the probability of high-O<sub>3</sub> events peaks, and increases with both  $\Omega_{NO_2}$  and  $\Omega_{HCHO}$ . While Figure 1a resembles this overall O<sub>3</sub>–NO<sub>x</sub>–VOC chemistry, the high O<sub>3</sub> probabilities span a broad range, with an uncertain, blurry transition between NO<sub>x</sub>-limited and VOC-limited regimes. The lack of sharp transitions between O<sub>3</sub> production regimes in Figure 1a likely reflects the influence from other factors such as varying meteorology, chemical and depositional loss of O<sub>3</sub>, noisy satellite retrievals, the spatial mismatch between the area satellite observations and the point measurements of surface O<sub>3</sub>, and in some cases, small sample size that lacks statistical power to calculate high-

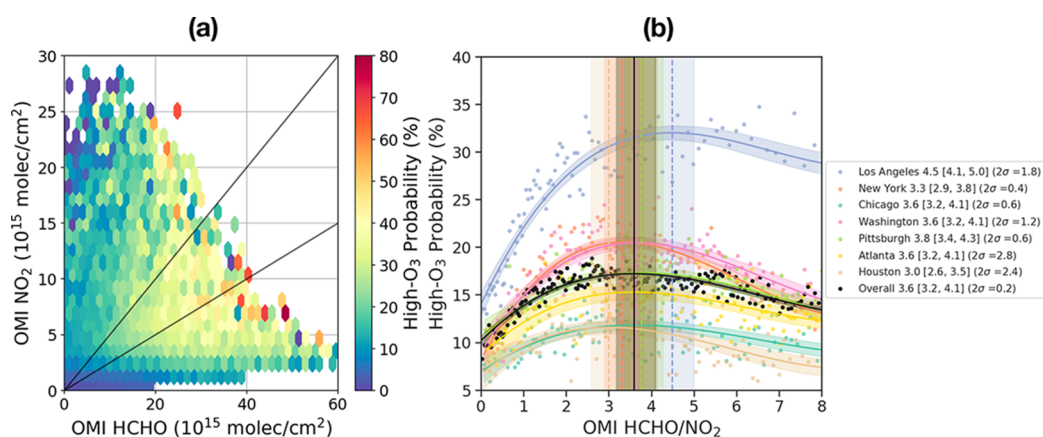


**Figure 1.** (a) Probability of O<sub>3</sub> exceeding 70 ppbv (high-O<sub>3</sub> probability) as a function of OMI  $\Omega_{\text{NO}_2}$  and  $\Omega_{\text{HCHO}}$ . All ground-based hourly O<sub>3</sub> observations (averaged at 1 PM and 2 PM local time) in the warm season (May to October) from 2005 to 2016 are aggregated based on corresponding daily OMI  $\Omega_{\text{NO}_2}$  and  $\Omega_{\text{HCHO}}$  (interval:  $0.5 \times 10^{15}$  molecules/cm<sup>2</sup>). We only include sites over polluted regions (defined as long-term average OMI  $\Omega_{\text{NO}_2} > 1.5 \times 10^{15}$  molecules/cm<sup>2</sup>). The probability is the number of observations with O<sub>3</sub> higher than 70 ppbv divided by the total number of observations at given OMI  $\Omega_{\text{NO}_2}$  and  $\Omega_{\text{HCHO}}$ . The black lines delineate OMI HCHO/NO<sub>2</sub> values of 2 and 4. (b) Probability of O<sub>3</sub> exceeding 70 ppbv as a function of OMI HCHO/NO<sub>2</sub> for all selected sites (black) and seven cities individually. High-O<sub>3</sub> probability is calculated by first matching hourly O<sub>3</sub> observations with daily OMI HCHO/NO<sub>2</sub>, dividing these paired observations to 100 (200 for black dots) bins based on OMI HCHO/NO<sub>2</sub>, and then calculating the high-O<sub>3</sub> probability (*y* axis) for each OMI HCHO/NO<sub>2</sub> bin (*x* axis, labeled as a dot). The solid lines are fitted third order polynomial curves, and the shading indicates 95% confidence intervals. The vertical lines indicate the maximum of the fitted curve (labeled in the legend), and the vertical shading represents the range over the top 10% of the fitted curve (regime transition). The uncertainty is two standard deviation (2 $\sigma$  or 95% confidence interval) of the derived peaks using statistical bootstrapping by iteratively running the model on 50 randomly selected subsets of 30 data pairs.

O<sub>3</sub> probability. Despite these uncertainties, Figure 1a qualitatively illustrates the nonlinear relationship between the occurrence probability of high-O<sub>3</sub> events and the HCHO and NO<sub>2</sub> proxies for precursor VOC and NO<sub>x</sub>, respectively.

Having established this qualitative approach, we next derive quantitative relationships by calculating high-O<sub>3</sub> probabilities at given OMI HCHO/NO<sub>2</sub> and examining their statistical relationship across different U.S. cities. We investigate three possible empirical relationships by applying moving average, second-order polynomial and third-order polynomial models to observations over seven U.S. cities (Figure S6). The third-order polynomial model is used to derive the maximum high-O<sub>3</sub> probability (the peak of the curve in Figure 1b), because it best fits the data, with the smallest uncertainty (estimated with statistical bootstrapping, Figure S6) and higher correlation coefficient (*R*) than the second-order model. Assuming that the peak of the curve marks the transition from VOC-limited to NO<sub>x</sub>-limited regime,<sup>56</sup> we define the transitional regime as the range of HCHO/NO<sub>2</sub> spanning the top 10% of the high-O<sub>3</sub> probability distribution.

Aggregating over all available observations used in Figure 1a, we find that the high-O<sub>3</sub> probability peaks at HCHO/NO<sub>2</sub> = 3.6, with the transitional regime ranging from 3.2 to 4.1, hereafter denoted as [3.2, 4.1]. Evaluating the relationship for the seven cities individually, we find robust nonlinear relationships between the high-O<sub>3</sub> probability and OMI HCHO/NO<sub>2</sub>, despite differences in the overall high-O<sub>3</sub> probability, which reflect other factors such as emissions, meteorology, and transport. The HCHO/NO<sub>2</sub> marking the regime transition varies slightly among these cities, which is highest for LA (4.5 [4.1, 5.0]), and lowest for Houston (3.0 [2.6, 3.5]). We evaluate the uncertainty in the derived peaks using statistical bootstrapping by iteratively applying the model to 50 randomly selected subsets of the data. We define the uncertainty as two standard deviations (2 $\sigma$  or 95% confidence

interval) from the derived maxima. The uncertainty is generally within 2 except for Atlanta (2 $\sigma$  = 2.8) and Houston (2 $\sigma$  = 2.4), where the fitted curve is relatively flat. Separating the observations into two periods (before and after 2009), the derived thresholds are slightly higher in the later period, which may reflect more high HCHO/NO<sub>2</sub> values in the recent period, driving the curve to move toward a higher turning point, but the uncertainty also increases as we halve the number of observations (Figure S7).

The HCHO/NO<sub>2</sub> thresholds derived in Figure 1b are higher than previously reported model-based values,<sup>16,17,19</sup> implying that at the same HCHO/NO<sub>2</sub>, our observation-based approach suggests O<sub>3</sub> production is more VOC-limited. The difference originates from the distinct approaches used to link HCHO/NO<sub>2</sub> with O<sub>3</sub> production regimes. Previous modeling studies derive the threshold by simulating the response of surface O<sub>3</sub> to an overall reduction in NO<sub>x</sub> or NMVOC emissions with coarse resolution models, which best capture regional as opposed to local O<sub>3</sub>-NO<sub>x</sub>-VOC sensitivity.<sup>16,19</sup> Our thresholds derived with in situ observations should be more indicative of the local O<sub>3</sub> chemistry, including the effect of NO<sub>x</sub> titration over urban areas. Schroeder et al.<sup>21</sup> also found VOC-limited chemistry occurring at high HCHO/NO<sub>2</sub> (1.3–5.0) in their analysis of column HCHO/NO<sub>2</sub> from aircraft measurements.

**Declining NO<sub>2</sub> Over Time.** Figure 2a shows summertime average  $\Omega_{\text{NO}_2}$  over seven metropolitan areas in 1996–2000 versus 2013–2016 produced from the harmonized multi-satellite data. NO<sub>2</sub> is concentrated over urban areas and near combustion sources. Applying the resolution corrections to GOME NO<sub>2</sub> reveals spatial gradients not detected directly with the coarse resolution of GOME (Figure S8). We find the largest urban–rural gradients in NYC and LA, where  $\Omega_{\text{NO}_2}$  varies by a factor of 10 within their core-based statistical areas (CBSA, outlined in Figure 2). Satellite observations show large

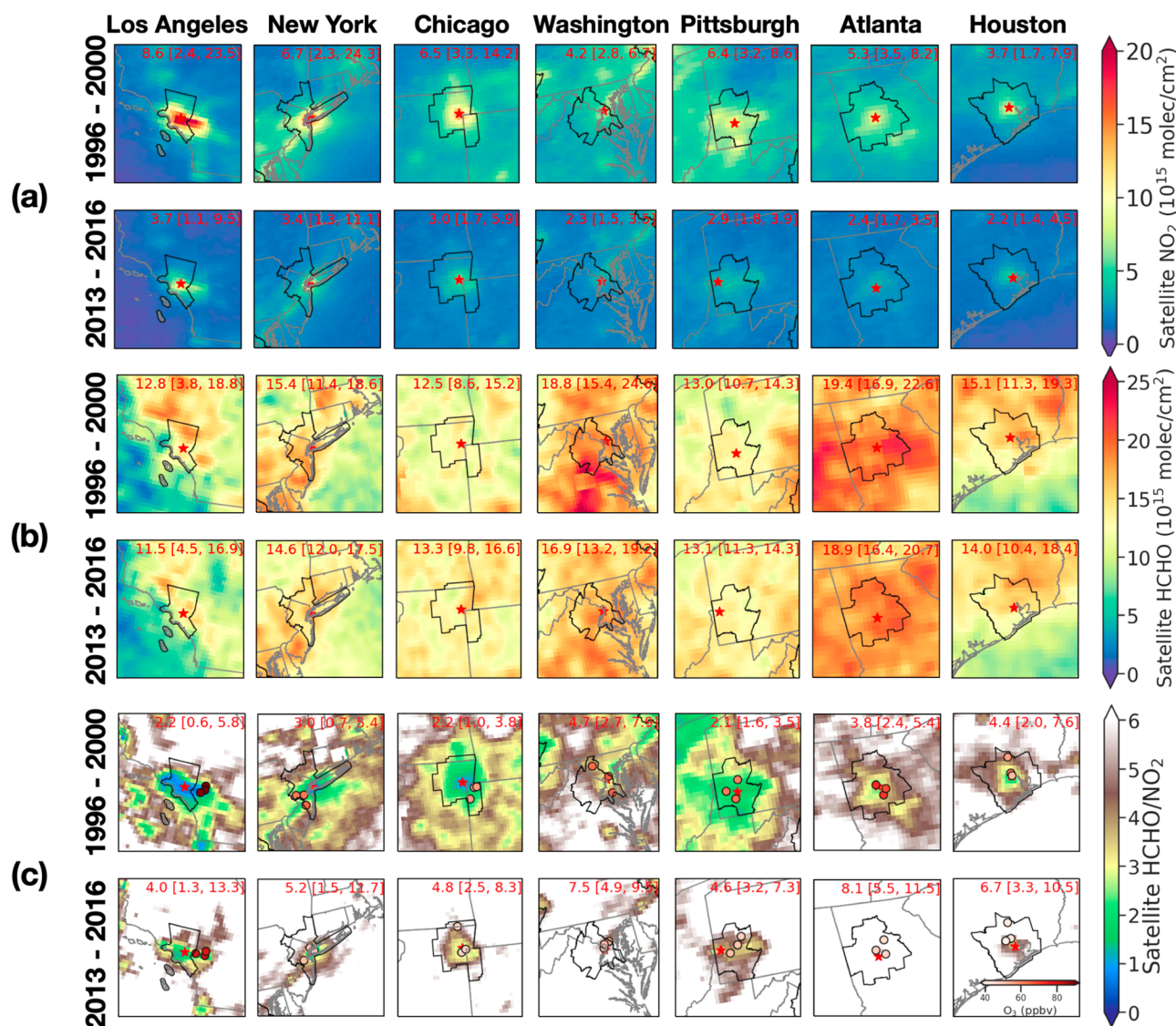


**Figure 2.** Maps of satellite-based summertime average: (a)  $\Omega_{\text{NO}_2}$ , (b)  $\Omega_{\text{HCHO}}$ , and (c) HCHO/NO<sub>2</sub> for seven cities (New York, Los Angeles, Chicago, Washington, DC, Pittsburgh, Atlanta, and Houston) in 1996–2000 and 2013–2016. The white area in (c) indicates HCHO/NO<sub>2</sub> above 6. The numbers show the mean and the range of  $\Omega_{\text{NO}_2}$ ,  $\Omega_{\text{HCHO}}$ , and HCHO/NO<sub>2</sub> for each core-based statistical area (CBSA, outlined in black). The red star shows the location with highest  $\Omega_{\text{NO}_2}$  in the CBSA. The red circles in the bottom two rows label the locations of three AQS sites where the highest O<sub>3</sub> occurred in the region, and the color represents the summertime mean O<sub>3</sub> (color bar inset in bottom right panel). Maps for 2001–2004, 2005–2008, and 2009–2012 are shown in Figure S11.

decreases in  $\Omega_{\text{NO}_2}$  over the past two decades, consistent with previous studies (Figure 2a).<sup>7,52,58</sup> The mean  $\Omega_{\text{NO}_2}$  in each CBSA has decreased by 40% (Atlanta) to 56% (LA) in 2013–2016 relative to 1996–2000. We use ground-based measurements of NO<sub>x</sub> to evaluate the long-term changes of satellite-based  $\Omega_{\text{NO}_2}$ , since our approach assumes  $\Omega_{\text{NO}_2}$  is a good indicator of ground-level NO<sub>x</sub>. Satellite-based  $\Omega_{\text{NO}_2}$  captures the decrease of ground-level NO<sub>x</sub> over LA, Chicago, and Washington to within 5%, but underestimates the decrease over NYC, Pittsburgh, and Houston, while overestimating the decreases in Atlanta (Figure S9). Both satellite-based  $\Omega_{\text{NO}_2}$  and ground-level NO<sub>x</sub> show the largest decline before 2004 over Pittsburgh, associated with emission controls on coal-fired power plants.<sup>59,60</sup> Satellite-based  $\Omega_{\text{NO}_2}$  does not show decreases over NYC and Houston before 2000, but ground-based NO<sub>x</sub> suggests large decreases (Figure S10). This discrepancy is likely due to the coarse resolution of GOME;

while we have corrected the spatial patterns of GOME  $\Omega_{\text{NO}_2}$ , the total  $\Omega_{\text{NO}_2}$  may still be biased low, due to the contributions from the nearby ocean where NO<sub>2</sub> is low. Satellite-based  $\Omega_{\text{NO}_2}$  does capture the large decreases between 2005 and 2012 in NYC and Houston (Figure S10). Over LA, Chicago, Washington, and Atlanta, both satellite and ground-based observations suggest the largest reductions occurred between 2005 to 2012 (Figure S10), when emission controls on power plants and stricter vehicle emission standards were implemented.<sup>26,61</sup> The substantial decrease in 2008–2010 may also reflect the economic recession.<sup>7,61</sup> In the most recent period (2013–2016), satellite data show flattening trends in  $\Omega_{\text{NO}_2}$  in all seven cities (Figure S10), possibly related to a slowdown of NO<sub>x</sub> emission reductions,<sup>29</sup> changes in NO<sub>x</sub> lifetime,<sup>28</sup> and the relatively larger influence of upper tropospheric NO<sub>2</sub> as anthropogenic contributions decline.<sup>22</sup>

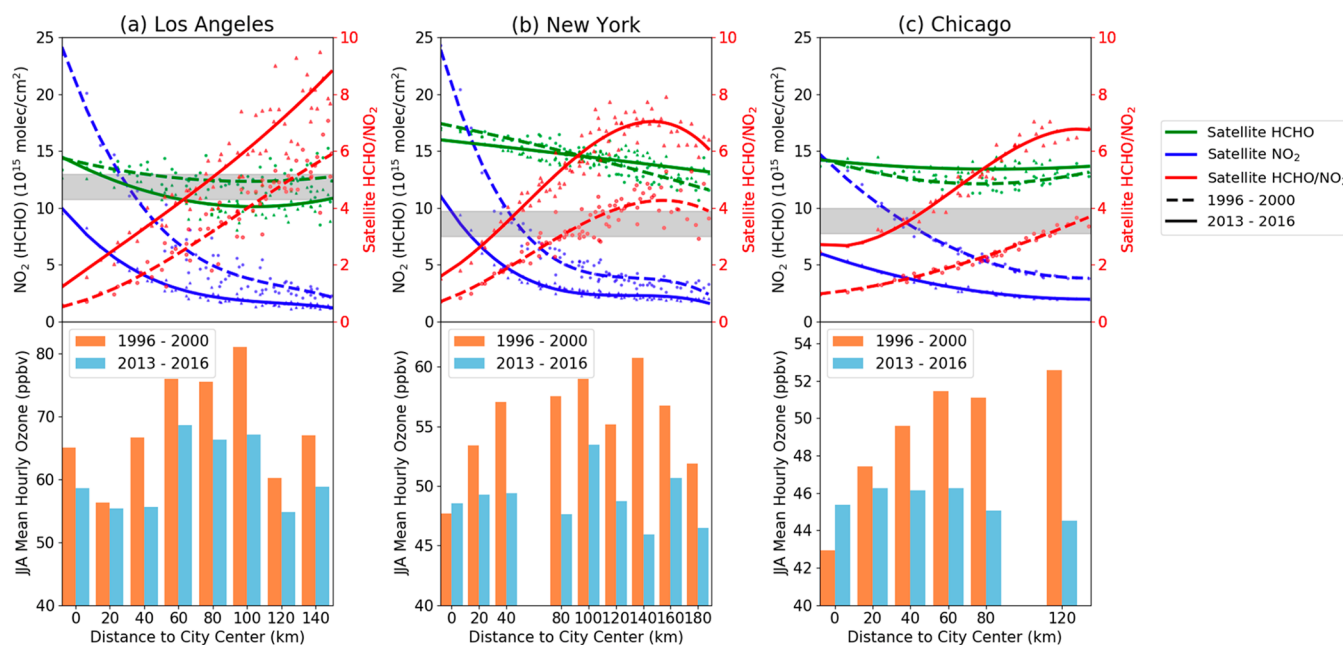


**Figure 3.** Satellite-based summertime  $\Omega_{\text{NO}_2}$  (blue dots),  $\Omega_{\text{HCHO}}$  (green dots), HCHO/NO<sub>2</sub> (red dots), and summertime average O<sub>3</sub> (bars) as a function of distance to the city center during 1996–2000 and 2013–2016 for three cities: (a) Los Angeles, (b) New York, and (c) Chicago. City center is defined as the grid cell with highest summertime  $\Omega_{\text{NO}_2}$  within this region (labeled as red stars in Figure 2), which we find does not change over time in these cities (Figures 2 and S11). The curves shown in the top row are a polynomial fit (third order for  $\Omega_{\text{NO}_2}$  and HCHO/NO<sub>2</sub>, second order for  $\Omega_{\text{HCHO}}$ ) curves. The gray area indicates the regime transitions for HCHO/NO<sub>2</sub>, which is derived for each city individually as shown in Figure 1b. Summertime average O<sub>3</sub> is calculated from hourly AQS observations at OMI overpass time (averaged at 1 PM and 2 PM local time). AQS O<sub>3</sub> sites are grouped by distance to the city center at 20 km intervals.

**Heterogeneous Trends of HCHO.** Figure 2b compares summertime multisatellite  $\Omega_{\text{HCHO}}$  in 1996–2000 versus 2013–2016. The spatial patterns of HCHO over the U.S. are largely driven by variations in biogenic VOCs, especially isoprene, which is mainly emitted from broadleaf trees, and is most abundant in the southeastern U.S.A.<sup>53</sup> As expected, the mean  $\Omega_{\text{HCHO}}$  is highest over the southeastern city of Atlanta, followed by Washington and NYC.  $\Omega_{\text{HCHO}}$  shows strong interannual variability (Figure S12), driven by interannual variability of meteorology, temperature in particular.<sup>55,62</sup> Over urban areas, satellite-based  $\Omega_{\text{HCHO}}$  decreased by 7% in LA, 4% in NYC, 3% in Pittsburgh, 4% in Atlanta, and 3% in Houston in 2013–2016 relative to 1996–2000 (Figure S9), consistent with the widespread reduction of anthropogenic VOC emissions.<sup>25</sup> Over surrounding rural areas, satellite-based  $\Omega_{\text{HCHO}}$  decreased near LA, Washington, Atlanta, and Houston, but increased near New York, Chicago, and Pittsburgh. These changes in  $\Omega_{\text{HCHO}}$  correspond to estimated long-term changes in isoprene emissions (Figure S13), which have previously been shown to be related to changes in vegetation coverage.<sup>63</sup> In addition, NO<sub>x</sub> reductions could lead to lower the HCHO yield from isoprene oxidation,<sup>64,65</sup> but the available observations are insufficient to conclusively determine the changes in HCHO yield. Overall, long-term changes in HCHO are driven by several factors,<sup>66</sup> such as anthropogenic and biogenic emissions, OH abundance, and HCHO yield dependence on NO<sub>x</sub>, which warrant further investigation as more measurements become more available.<sup>67</sup> Most relevant to our study is that the overall changes in HCHO are much smaller than the NO<sub>2</sub> changes over the last two decades (Figure 2).

**Spatial Expansion of NO<sub>x</sub>-limited Regime Over Time.** As  $\Omega_{\text{NO}_2}$  decreased over time, while changes in  $\Omega_{\text{HCHO}}$  were relatively small, satellite-based HCHO/NO<sub>2</sub> increased from

1996–2000 to 2013–2016, indicating a shrinking extent of NO<sub>x</sub>-saturated O<sub>3</sub> formation in urban areas (Figure 2c). Using the thresholds derived from Figure 1b to identify the O<sub>3</sub> production regimes, NO<sub>x</sub>-saturated chemistry existed during summer in all cities during 1996–2000, with the largest areal extent in Pittsburgh. By 2013–2016, NO<sub>x</sub>-saturated chemistry only occurred in the center of LA, Chicago, and NYC. The spatial expansion of the NO<sub>x</sub>-limited regime suggests that NO<sub>x</sub> emission reductions are more effective today at reducing O<sub>3</sub> pollution, as confirmed from prior modeling<sup>35,36,68</sup> and ground-based observational studies.<sup>34,56</sup> In recent years, as  $\Omega_{\text{NO}_2}$  remains at low levels,  $\Omega_{\text{HCHO}}$  plays a more important role in determining the spatial and temporal variability in HCHO/NO<sub>2</sub>. For example, the mean  $\Omega_{\text{HCHO}}$  over LA is  $8.2 \times 10^{15}$  molecules/cm<sup>2</sup> in 2010, but increases to  $15.2 \times 10^{15}$  molecules/cm<sup>2</sup> in 2011, leading the mean O<sub>3</sub> formation regime to shift from NO<sub>x</sub>-saturated to NO<sub>x</sub>-limited (Figure S14). Also, Atlanta and Pittsburgh show similar  $\Omega_{\text{NO}_2}$  in 2013–2016, but  $\Omega_{\text{HCHO}}$  is 50% higher in Atlanta, leading to 76% higher HCHO/NO<sub>2</sub> and thus more NO<sub>x</sub>-limited chemistry in Atlanta, consistent with the well-understood regional differences in summertime O<sub>3</sub> sensitivity.<sup>69,70</sup>

LA, NYC, and Chicago are the three cities where we find strong urban–rural gradients in HCHO/NO<sub>2</sub>, where O<sub>3</sub> production transitions from NO<sub>x</sub>-saturated at city centers toward a NO<sub>x</sub>-limited regime over rural areas in both periods. Figure 3 shows summertime average satellite-based NO<sub>2</sub>, HCHO, and HCHO/NO<sub>2</sub> as a function of the distance to the city center during 1996–2000 and 2013–2016 over these three cities. Satellite observations detect large urban–rural gradients of NO<sub>2</sub> in LA and NYC with  $20 \times 10^{13}$  molecules/cm<sup>2</sup>/km in 1996–2000, which decrease to  $8 \times 10^{13}$  molecules/cm<sup>2</sup>/km in 2013 to 2016. The urban–rural gradient has

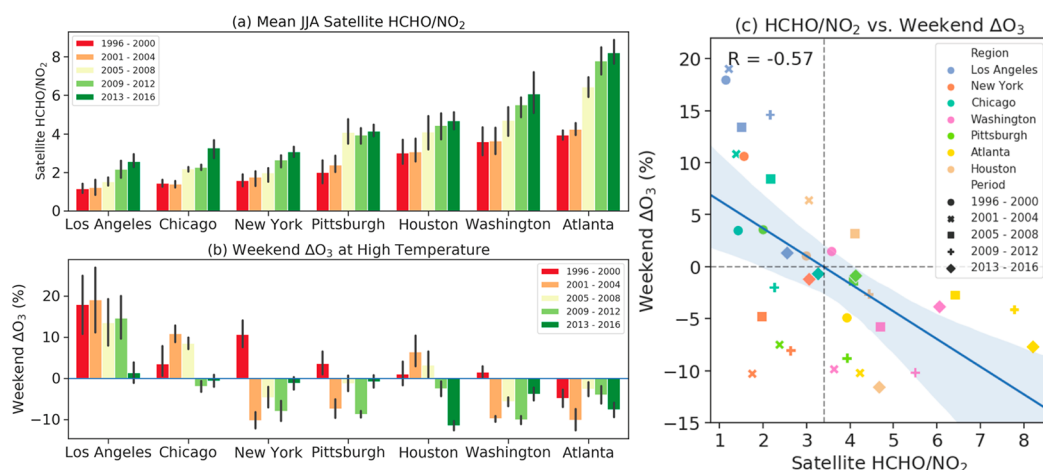


**Figure 4.** (a) Satellite-based summertime average HCHO/NO<sub>2</sub> in seven cities during five periods. (b) Weekday-to-weekend difference in average 1–2 pm summertime O<sub>3</sub> (weekend ΔO<sub>3</sub>, mean O<sub>3</sub> Saturday–Sunday minus mean O<sub>3</sub> Tuesday–Friday) within each city on high temperature days (>median summer average temperature 1–2 pm) observed at AQS sites during five periods. Satellite-based HCHO/NO<sub>2</sub> is sampled over ground-based AQS O<sub>3</sub> sites. The error bars represent year-to-year variability in a given period. (c) Scatter plot between summertime average satellite-based HCHO/NO<sub>2</sub> and the weekend ΔO<sub>3</sub> with colors representing different cities and symbols representing different periods. The blue line is the fitted linear regression line with the 95% confidence interval shaded.

decreased from  $11 \times 10^{13}$  molecules/cm<sup>2</sup>/km to  $3 \times 10^{13}$  molecules/cm<sup>2</sup>/km in Chicago. We find a small enhancement of  $\Omega_{\text{HCHO}}$  in urban areas over NYC and LA of  $2$  to  $3 \times 10^{13}$  molecules/cm<sup>2</sup>/km, and negligible urban–rural difference of  $\Omega_{\text{HCHO}}$  in Chicago. The urban–rural gradient of OMI HCHO/NO<sub>2</sub> is therefore mainly driven by the variations in NO<sub>2</sub>. Using the regime thresholds we estimated, we infer the regime transition occurred at 110 to 130 km away from the city center in LA, 80 to 120 km in NYC, and 120 to 130 km in Chicago in 1996–2000. By 2013–2016, the locations of regime transition have moved closer to the city centers: 50 to 70 km for LA, 40 to 60 km for NYC and 30 to 60 km for Chicago (Figure 3).

**Observed Response of Ground-Level O<sub>3</sub> to Regime Transitions.** Theoretically, O<sub>3</sub> production regime transitions should correspond to the conditions at which O<sub>3</sub> formation is most efficient.<sup>57</sup> As the regime transition moves closer to populated city centers, peak O<sub>3</sub> production efficiency is expected to move toward the city center. We hypothesize that we should observe the highest O<sub>3</sub> concentration where the transitional regime occurs, assuming that local changes in meteorology, chemical and depositional loss do not contribute strongly to the observed summertime mean urban-to-rural O<sub>3</sub> gradients. We find that the ground-based sites measuring the highest summertime mean O<sub>3</sub> in each region move toward the city centers over time, except for Atlanta and Houston, where the highest O<sub>3</sub> is found near the city center in both periods (Figure 2c). We aggregate ground-based O<sub>3</sub> sites based on their distance to the city center for LA, NYC, and Chicago (Figure 3), where the VOC-limited regime still existed in 2013–2016. As expected, peak O<sub>3</sub> has moved toward the city center from 1996–2000 to 2013–2016 in LA and Chicago: from ~100 km to ~60 km in LA, from 120 km to 20 km in Chicago. The locations of peak O<sub>3</sub> are largely consistent with the locations of the regime transition identified by the satellite-based HCHO/NO<sub>2</sub>. In NYC, we find that O<sub>3</sub> peaks ~140 km away in 1996–2000, which is consistent with the regime transition inferred from satellite-based HCHO/NO<sub>2</sub>. In 2013–2016, O<sub>3</sub> shows peaks at 100 and 160 km, however, which may be due to the noncircular nature of city shape and possibly

confounding role of nearby ocean. If we only consider the small region within 100 km, then O<sub>3</sub> peaks at 40 km away from the city center, more consistent with the regime transition inferred from satellite-based HCHO/NO<sub>2</sub>.

Regionally, surface O<sub>3</sub> in summer has decreased over the past two decades over the U.S.A., especially over the eastern U.S.A.<sup>30,33,71,72</sup> As expected, summertime mean O<sub>3</sub> is smaller in 2013–2016 than 1996–2000 over the three megacities, but the reduction is larger over rural areas where O<sub>3</sub> formation falls in the NO<sub>x</sub>-limited regime (Figure 3). The faster decline in O<sub>3</sub> over rural areas than urban areas has previously been demonstrated.<sup>33</sup> In NYC and Chicago, we find an increase in O<sub>3</sub> at the city center where O<sub>3</sub> formation is NO<sub>x</sub>-saturated. In the NO<sub>x</sub>-saturated regime, NO<sub>x</sub> emission reductions decrease NO<sub>x</sub> titration, which increases O<sub>3</sub> directly, and also increases OH available for VOC oxidation and subsequent O<sub>3</sub> production. The spatial difference between maximum and minimum O<sub>3</sub> narrows from 13 ppbv in 1996–2000 to 7 ppbv in 2013–2016 in NYC, and 10 ppbv to 2 ppbv in Chicago. In LA, O<sub>3</sub> decreases in urban areas, which we attribute to decreases in anthropogenic VOC emissions.<sup>73</sup> The largest O<sub>3</sub> decreases occur in the transitional regimes in LA, where reductions in both anthropogenic VOCs and NO<sub>x</sub> lower O<sub>3</sub>.

**Reversal of the O<sub>3</sub> Weekend Effect.** The decrease of urban NO<sub>x</sub> emissions associated with road traffic on weekends provides an observation-based natural test for investigating O<sub>3</sub> sensitivity to NO<sub>x</sub> emissions;<sup>74,75</sup> over urban areas where O<sub>3</sub> formation is NO<sub>x</sub>-saturated, reduction of NO<sub>x</sub> emissions on weekends increases in O<sub>3</sub> (referred to as the O<sub>3</sub> weekend effect). Figure 4 shows the mean satellite-based HCHO/NO<sub>2</sub> sampled over long-term O<sub>3</sub> sites for the seven selected cities in five periods, and the corresponding in situ observed weekday-to-weekend difference in average summertime O<sub>3</sub> (weekend ΔO<sub>3</sub>) within each metropolitan area. Here we only select days with high temperature (>median summertime average), as they are generally associated with high pressure, clearer skies, and slower winds, conditions suitable for efficient O<sub>3</sub> production.<sup>37,57</sup> As O<sub>3</sub> production becomes more sensitive to NO<sub>x</sub>, the weekend ΔO<sub>3</sub> lessens and even reverses in some cities. The extent of the NO<sub>x</sub>-saturated regime is largest in LA, as

suggested by the lowest average satellite HCHO/NO<sub>2</sub> (Figure 4a). The O<sub>3</sub> weekend effect in LA persists from 1996 to 2016, but is smallest in the most recent period. During 1996–2000, we find a positive weekend  $\Delta O_3$  in 18 (11 with  $p < 0.1$ ) out of 20 sites along southern California (Figure S15), but only 11 out of 18 sites (5 with  $p < 0.1$ ) during 2013–2016. The shrinking O<sub>3</sub> weekend effect after 2000 in LA is reported in previous studies.<sup>76,77</sup> Chicago has the second lowest HCHO/NO<sub>2</sub>, and the weekend  $\Delta O_3$  changes from positive to negative in 2009–2012. Over Chicago, the O<sub>3</sub> weekend effect is strongest during 2001–2004, when 32 out of 34 sites show positive weekend  $\Delta O_3$ , and diminishes to 10 out of 23 sites during 2013–2016 (Figure S15). The reversal of the O<sub>3</sub> weekend effect occurs earlier in 2001–2004 over NYC, Pittsburgh, and Washington, though satellite HCHO/NO<sub>2</sub> does not change much compared with 1996–2000. In Houston, we find the reversal of weekend  $\Delta O_3$  occurs around 2009–2012. In Houston, 17 out of 24 sites show positive weekend  $\Delta O_3$  during 2001–2004, but they all changed sign during 2013–2016 (Figure S15). In Atlanta, where O<sub>3</sub> formation is most NO<sub>x</sub>-limited based on our metric, O<sub>3</sub> concentration remains lower on weekends than weekdays at high temperature, but a reversal of the O<sub>3</sub> weekend effect does occur at moderate temperature during 2005–2008 (Figure S16).

The observed long-term changes in the O<sub>3</sub> weekend effect are overall consistent with the increasing sensitivity to NO<sub>x</sub> as suggested by the increasing satellite-based HCHO/NO<sub>2</sub> (Figure 4a). We find that satellite-based HCHO/NO<sub>2</sub> and weekend  $\Delta O_3$  is moderately correlated ( $R = -0.57$ ,  $p < 0.001$ , Figure 4c). The regression line intercepts 0 at HCHO/NO<sub>2</sub> = 3.4, which is close to the regime transition derived in Figure 1b. Using this satellite-based indicator to quantitatively predict the occurrence of O<sub>3</sub> weekend effect in any particular city for a given time period, however, is subject to uncertainties. The definition of the O<sub>3</sub> weekend effect we invoke here assumes that the only difference in O<sub>3</sub> is directly attributable to changes in NO<sub>x</sub> emission. The observed O<sub>3</sub> differences, however, may also be influenced by variability in meteorology.<sup>42,78</sup> The early reversal of the O<sub>3</sub> weekend effect in 2001–2004 over northeastern cities (NYC, Washington and Pittsburgh) is better explained by the overall colder temperature on weekends than weekdays over these three cities (Figure S17). Pierce et al.<sup>42</sup> suggest the long-term trend in the O<sub>3</sub> weekend effect over the Northeast U.S.A. is strongly influenced by the interannual variability in meteorology. We find larger fluctuations of the weekend  $\Delta O_3$  at moderate temperatures in most cities except for LA (Figure S16), which may be related to meteorological conditions that act to weaken urban-to-rural gradients through regional-scale O<sub>3</sub> transport that dilutes the signal of local urban O<sub>3</sub> production.

**Limitations and Future Directions.** Our study is the first attempt to directly connect satellite-based HCHO/NO<sub>2</sub> with ground-based O<sub>3</sub> observations. We show that space-based HCHO/NO<sub>2</sub> captures the nonlinearities of O<sub>3</sub>–NO<sub>x</sub>–VOC chemistry and detects spatial expansion of the NO<sub>x</sub>-limited regime as supported by ground-based observations. However, using satellite HCHO/NO<sub>2</sub> to quantitatively diagnose the effectiveness of emission controls is subject to the following uncertainties that warrant further investigation. First, theoretical studies that relate indicator ratio to O<sub>3</sub>–NO<sub>x</sub>–VOC sensitivity show variations among different locations, which are subject to uncertainties in deposition and interactions with

aerosol.<sup>14,79</sup> Second, satellite instruments measure the vertically integrated column density, and inhomogeneities in vertical distributions degrade the ability of satellite-based column HCHO/NO<sub>2</sub> to identify the near-surface O<sub>3</sub> sensitivity.<sup>19,21</sup> Third, we use an empirical observation-based approach to derive the thresholds marking the transitions between chemical regimes, which are likely to be affected by not only biases in the satellite retrieval algorithms,<sup>19</sup> but also by sampling size and biases of both ground-based and space-based observations. Fourth, the extent to which satellite-based  $\Omega_{\text{HCHO}}$  relates to local surface organic reactivity is unclear. Satellite-based  $\Omega_{\text{HCHO}}$  shows small decreasing trends over urban areas, and are mostly insensitive to observed decreases in anthropogenic VOCs,<sup>56,73</sup> partially due to relatively small HCHO yields from some classes of anthropogenic VOCs (e.g., alkanes).<sup>80</sup> As HCHO is a weaker UV–visible absorber than NO<sub>2</sub>, satellite retrieval of HCHO is more prone to errors,<sup>46</sup> which may limit its ability to detect HCHO from local sources of anthropogenic VOCs. We find small enhancements of satellite  $\Omega_{\text{HCHO}}$  over urban areas, but the magnitudes of the enhancement are insensitive to resolution, suggesting satellite  $\Omega_{\text{HCHO}}$  is more indicative of the regional VOC reactivity, which is mainly influenced by biogenic isoprene emissions across much of the U.S.A. in summer.<sup>81</sup> Finally, although the retrieval uncertainty associated with different instruments has largely been reduced in the QA4ECV products,<sup>49</sup> our applications of satellite-based HCHO/NO<sub>2</sub> are nonetheless limited to long-term averages or data aggregations of sufficiently large sample size to reduce retrieval noise. It is challenging to use current satellite retrievals to observe short-term variability and detailed spatial patterns within urban cores. The new generation of satellites, including the newly launched TROPOMI aboard Sentinel-5P, and the upcoming geostationary satellite instruments such as TEMPO will offer an unprecedented view to characterize the near-surface O<sub>3</sub> chemistry at finer spatial and temporal scales.<sup>82,83</sup>

## ■ ASSOCIATED CONTENT

### SI Supporting Information

The Supporting Information is available free of charge at <https://pubs.acs.org/doi/10.1021/acs.est.9b07785>.

S1, Details on satellite retrieval of NO<sub>2</sub> and HCHO; S2, gridding of satellite products; S3, discussion on the choice of resolution; Figure S1, difference between OMI and SCIAMACHY  $\Omega_{\text{NO}_2}$ ; Figure S2, resolution correction factor for  $\Omega_{\text{NO}_2}$ ; Figure S3, year-to-year variability in  $\text{RC}_{\text{NO}_2\text{-OMI}}$ ; Figure S4, temporal correlation between  $\text{RC}_{\text{NO}_2\text{-OMI}}$  and  $\text{RC}_{\text{NO}_2\text{-SCIA}}$ ; Figure S5, resolution correction of OMI  $\Omega_{\text{HCHO}}$  and systematic difference between OMI and SCIAMACHY  $\Omega_{\text{HCHO}}$ ; Figure S6, Figure 1b for comparison of multiple models; Figure S7, Figure 1b for comparison of two periods; Figure S8, resolution corrected versus original GOME  $\Omega_{\text{NO}_2}$ ; Figure S9, relative changes in summertime average satellite-based  $\Omega_{\text{NO}_2}$  and ground-based measurements of NO<sub>x</sub>,  $\Omega_{\text{HCHO}}$  over urban and rural areas; Figure S10, time series of satellite-based  $\Omega_{\text{NO}_2}$  and ground-based NO<sub>x</sub>; Figure S11, Figure 2 for the other three periods; Figure S12, time series of satellite-based  $\Omega_{\text{HCHO}}$ ; Figure S13, long-term changes in biogenic isoprene emissions; Figure S14, time series of satellite-based HCHO/NO<sub>2</sub>; Figure S15, maps of O<sub>3</sub> weekend



effect; Figure S16, Figure 4b for moderate temperature; and Figure S17, weekday-to-weekend difference in temperature. (PDF)

## AUTHOR INFORMATION

### Corresponding Author

**Xiaomeng Jin** – Department of Earth and Environmental Sciences, Columbia University, New York, New York 10027, United States; Lamont-Doherty Earth Observatory of Columbia University, Palisades, New York 10964, United States;  
orcid.org/0000-0002-6895-8464; Email: xjin@ldeo.columbia.edu

### Authors

**Arlene Fiore** – Department of Earth and Environmental Sciences, Columbia University, New York, New York 10027, United States; Lamont-Doherty Earth Observatory of Columbia University, Palisades, New York 10964, United States  
**K. Folkert Boersma** – Royal Netherlands Meteorological Institute, De Bilt 3730 AE, The Netherlands; Wageningen University, Environmental Sciences Group, Wageningen 6708 PB, The Netherlands  
**Isabelle De Smedt** – Belgian Institute for Space Aeronomy (BIRA-IASB), Brussels 1180, Belgium  
**Lukas Valin** – United States Environmental Agency, Office of Research and Development, Research Triangle Park, North Carolina 27709, United States

Complete contact information is available at:  
<https://pubs.acs.org/10.1021/acs.est.9b07785>

### Notes

The research presented was not performed or funded by EPA and was not subject to EPA's quality system requirements. The views expressed in this article are those of the authors and do not necessarily represent the views or the policies of the U.S. Environmental Protection Agency. The authors declare no competing financial interest.

## ACKNOWLEDGMENTS

Support for this project was provided by the NASA Earth and Space Science Fellowship (NESSF, Grant 80NSSC18K1399), and NASA Atmospheric Composition Modeling and Analysis Program (ACMAP, Grant NNX17AG40G). We acknowledge useful discussions with Bryan Duncan (NASA GSFC), Lok Lamsal (NASA GSFC), and Melanie Follette-Cook (Morgan State University).

## REFERENCES

- (1) Jerrett, M.; Burnett, R. T.; Pope, C. A. I.; Ito, K.; Thurston, G.; Krewski, D.; Shi, Y.; Calle, E.; Thun, M. Long-Term Ozone Exposure and Mortality. *N. Engl. J. Med.* **2009**, *360* (11), 1085–1095.
- (2) Cohen, A. J.; Brauer, M.; Burnett, R.; Anderson, H. R.; Frostad, J.; Estep, K.; Balakrishnan, K.; Brunekreef, B.; Dandona, L.; Dandona, R.; et al. Estimates and 25-Year Trends of the Global Burden of Disease Attributable to Ambient Air Pollution: An Analysis of Data from the Global Burden of Diseases Study 2015. *Lancet* **2017**, *389* (10082), 1907–1918.
- (3) Kleinman, L. I. Low and High Nox Tropospheric Photochemistry. *J. Geophys. Res.* **1994**, *99* (D8), 16831–16838.
- (4) Sillman, S.; Logan, J. A.; Wofsy, S. C. The Sensitivity of Ozone to Nitrogen Oxides and Hydrocarbons in Regional Ozone Episodes. *J. Geophys. Res.* **1990**, *95* (D2), 1837–1851.
- (5) Martin, R. V.; Jacob, D. J.; Chance, K.; Kurosu, T.; Palmer, P. I.; Evans, M. J. Global Inventory of Nitrogen Oxide Emissions

Constrained by Space-Based Observations of NO<sub>2</sub> Columns. *J. Geophys. Res.* **2003**, *108* (D17), 955.

(6) Lamsal, L. N.; Krotkov, N. A.; Celarier, E. A.; Swartz, W. H.; Pickering, K. E.; Bucsela, E. J.; Gleason, J. F.; Martin, R. V.; Philip, S.; Irie, H.; Cede, A.; Herman, J.; Weinheimer, A.; Szykman, J. J.; Knepp, T. N. Evaluation of OMI Operational Standard NO<sub>2</sub> Column Retrievals Using in Situ and Surface-Based NO<sub>2</sub> Observations. *Atmos. Chem. Phys.* **2014**, *14* (21), 11587–11609.

(7) Lamsal, L. N.; Duncan, B. N.; Yoshida, Y.; Krotkov, N. A.; Pickering, K. E.; Streets, D. G.; Lu, Z. U.S. NO<sub>2</sub> Trends (2005–2013): EPA Air Quality System (AQS) Data versus Improved Observations from the Ozone Monitoring Instrument (OMI). *Atmos. Environ.* **2015**, *110* (C), 130–143.

(8) Palmer, P. I.; Jacob, D. J.; Fiore, A. M.; Martin, R. V.; Chance, K. V.; Kurosu, T. P. Mapping isoprene emissions over North America using formaldehyde column observations from space. *J. Geophys. Res.* **2003**, *108* (D6), 155.

(9) Fu, T.-M.; Jacob, D. J.; Palmer, P. I.; Chance, K.; Wang, Y. X.; Barletta, B.; Blake, D. R.; Stanton, J. C.; Pilling, M. J. Space-Based Formaldehyde Measurements as Constraints on Volatile Organic Compound Emissions in East and South Asia and Implications for Ozone. *J. Geophys. Res.* **2007**, *112* (D6), D06312.

(10) Millet, D. B.; Jacob, D. J.; Boersma, K. F.; Fu, T.-M.; Kurosu, T. P.; Chance, K.; Heald, C. L.; Guenther, A. Spatial Distribution of Isoprene Emissions from North America Derived from Formaldehyde Column Measurements by the OMI Satellite Sensor. *J. Geophys. Res.* **2008**, *113* (D2), D02307.

(11) Marais, E. A.; Jacob, D. J.; Kurosu, T. P.; Chance, K.; Murphy, J. G.; Reeves, C.; Mills, G.; Casadio, S.; Millet, D. B.; Barkley, M. P.; Paulot, F.; Mao, J. Isoprene Emissions in Africa Inferred from OMI Observations of Formaldehyde Columns. *Atmos. Chem. Phys.* **2012**, *12* (14), 6219–6235.

(12) Zhu, L.; Jacob, D. J.; Mickley, L. J.; Marais, E. A.; Cohan, D. S.; Yoshida, Y.; Duncan, B. N.; Gonzalez Abad, G.; Chance, K. V. Anthropogenic Emissions of Highly Reactive Volatile Organic Compounds in Eastern Texas Inferred from Oversampling of Satellite (OMI) Measurements of HCHO Columns. *Environ. Res. Lett.* **2014**, *9* (11), 114004–114008.

(13) Shen, L.; Jacob, D. J.; Zhu, L.; Zhang, Q.; Zheng, B.; Sulprizio, M. P.; Li, K.; De Smedt, I.; Gonzalez Abad, G.; Cao, H.; Fu, T.-M.; Liao, H. The 2005–2016 Trends of Formaldehyde Columns Over China Observed by Satellites: Increasing Anthropogenic Emissions of Volatile Organic Compounds and Decreasing Agricultural Fire Emissions. *Geophys. Res. Lett.* **2019**, *46* (8), 4468–4475.

(14) Sillman, S. The Use of NO<sub>y</sub>, H<sub>2</sub>O<sub>2</sub>, and HNO<sub>3</sub> as Indicators for Ozone-NO<sub>x</sub>-hydrocarbon Sensitivity in Urban Locations. *J. Geophys. Res.* **1995**, *100* (D7), 14175–14188.

(15) Tonnesen, G. S.; Dennis, R. L. Analysis of Radical Propagation Efficiency to Assess Ozone Sensitivity to Hydrocarbons and NO<sub>x</sub>: 2. Long-lived Species as Indicators of Ozone Concentration Sensitivity. *J. Geophys. Res.* **2000**, *105* (D7), 9227–9241.

(16) Martin, R. V.; Fiore, A. M.; van Donkelaar, A. Space-Based Diagnosis of Surface Ozone Sensitivity to Anthropogenic Emissions. *Geophys. Res. Lett.* **2004**, *31* (6), L06120.

(17) Duncan, B. N.; Yoshida, Y.; Olson, J. R.; Sillman, S.; Martin, R. V.; Lamsal, L.; Hu, Y.; Pickering, K. E.; Allen, D. J.; Retscher, C.; Crawford, J. H. Application of OMI Observations to a Space-Based Indicator of NO<sub>x</sub> and VOC Controls on Surface Ozone Formation. *Atmos. Environ.* **2010**, *44* (18), 2213–2223.

(18) Jin, X.; Holloway, T. Spatial and Temporal Variability of Ozone Sensitivity over China Observed from the Ozone Monitoring Instrument. *Journal of Geophysical Research: Atmospheres* **2015**, *120* (14), 7229–7246.

(19) Jin, X.; Fiore, A. M.; Murray, L. T.; Valin, L. C.; Lamsal, L. N.; Duncan, B.; Folkert Boersma, K.; De Smedt, I.; Abad, G. G.; Chance, K.; Tonnesen, G. S. Evaluating a Space-Based Indicator of Surface Ozone-NO<sub>x</sub>-VOC Sensitivity Over Midlatitude Source Regions and Application to Decadal Trends. *Journal of Geophysical Research: Atmospheres* **2017**, *122* (19), 10439.

- (20) Brown-Steiner, B.; Hess, P. G.; Lin, M. Y. On the Capabilities and Limitations of GCCM Simulations of Summertime Regional Air Quality: A Diagnostic Analysis of Ozone and Temperature Simulations in the US Using CESM CAM-Chem. *Atmos. Environ.* **2015**, *101* (C), 134–148.
- (21) Schroeder, J. R.; Crawford, J. H.; Fried, A.; Walega, J.; Weinheimer, A.; Wisthaler, A.; Müller, M.; Mikoviny, T.; Chen, G.; Shook, M.; Blake, D. R.; Tonnesen, G. S. New Insights into the Column CH<sub>2</sub>O/NO<sub>2</sub> Ratio as an Indicator of near-Surface Ozone Sensitivity. *Journal of Geophysical Research: Atmospheres* **2017**, *122* (16), 8885–8907.
- (22) Silvern, R. F.; Jacob, D. J.; Mickley, L. J.; Sulprizio, M. P.; Travis, K. R.; Marais, E. A.; Cohen, R. C.; Laughner, J. L.; Choi, S.; Joiner, J.; Lamsal, L. N. Using Satellite Observations of Tropospheric NO<sub>2</sub> Columns to Infer Long-Term Trends in US NO<sub>x</sub> Emissions: The Importance of Accounting for the Free Tropospheric NO<sub>2</sub> Background. *Atmos. Chem. Phys.* **2019**, *19* (13), 8863–8878.
- (23) Wang, K.; Yahya, K.; Zhang, Y.; Hogrefe, C.; Pouliot, G.; Knote, C.; Hodzic, A.; San Jose, R.; Perez, J. L.; Jimenez-Guerrero, P.; Baro, R.; Makar, P.; Bennartz, R. A Multi-Model Assessment for the 2006 and 2010 Simulations under the Air Quality Model Evaluation International Initiative (AQMEII) Phase 2 over North America: Part II. Evaluation of Column Variable Predictions Using Satellite Data. *Atmos. Environ.* **2015**, *115*, 587.
- (24) Zhu, L.; Jacob, D. J.; Kim, P. S.; Fisher, J. A.; Yu, K.; Travis, K. R.; Mickley, L. J.; Yantosca, R. M.; Sulprizio, M. P.; De Smedt, I.; et al. Observing Atmospheric Formaldehyde (HCHO) from Space: Validation and Intercomparison of Six Retrievals from Four Satellites (OMI, GOME2A, GOME2B, OMPS) with SEAC4RS Aircraft Observations over the Southeast US. *Atmos. Chem. Phys.* **2016**, *16* (21), 13477–13490.
- (25) US EPA. O. U. Air Pollutant Emissions Trends Data; <https://www.epa.gov/air-emissions-inventories/air-pollutant-emissions-trends-data>, 2018.
- (26) Duncan, B. N.; Lamsal, L. N.; Thompson, A. M.; Yoshida, Y.; Lu, Z.; Streets, D. G.; Hurwitz, M. M.; Pickering, K. E. A Space-Based, High-Resolution View of Notable Changes in Urban NO<sub>x</sub> Pollution around the World (2005–2014). *Journal of Geophysical Research: Atmospheres* **2016**, *121* (2), 976–996.
- (27) Georgoulas, A. K.; van der A, R. J.; Stammes, P.; Boersma, K. F.; Eskes, H. J. Trends and Trend Reversal Detection in 2 Decades of Tropospheric NO<sub>2</sub> Satellite Observations. *Atmos. Chem. Phys.* **2019**, *19* (9), 6269–6294.
- (28) Laughner, J. L.; Cohen, R. C. Direct Observation of Changing NO<sub>x</sub> Lifetime in North American Cities. *Science* **2019**, *366* (6466), 723–727.
- (29) Jiang, Z.; McDonald, B. C.; Worden, H.; Worden, J. R.; Miyazaki, K.; Qu, Z.; Henze, D. K.; Jones, D. B. A.; Arellano, A. F.; Fischer, E. V.; Zhu, L.; Boersma, K. F. Unexpected Slowdown of US Pollutant Emission Reduction in the Past Decade. *Proc. Natl. Acad. Sci. U. S. A.* **2018**, *115* (20), 5099–5104.
- (30) Chang, K.-L.; Petropavlovskikh, I.; Copper, O. R.; Schultz, M. G.; Wang, T. Regional Trend Analysis of Surface Ozone Observations from Monitoring Networks in Eastern North America, Europe and East Asia. *Elem. Sci. Anth* **2017**, *5* (0), 50.
- (31) Yan, Y.; Lin, J.; He, C. Ozone Trends over the United States at Different Times of Day. *Atmos. Chem. Phys.* **2018**, *18* (2), 1185–1202.
- (32) Blanchard, C. L.; Shaw, S. L.; Edgerton, E. S.; Schwab, J. J. Emission Influences on Air Pollutant Concentrations in New York State. I. Ozone. *Atmospheric Environment: X* **2019**, *3*, 100033.
- (33) Simon, H.; Reff, A.; Wells, B.; Xing, J.; Frank, N. Ozone Trends Across the United States over a Period of Decreasing NO<sub>x</sub> and VOC Emissions. *Environ. Sci. Technol.* **2015**, *49* (1), 186–195.
- (34) Blanchard, C. L.; Hidy, G. M. Ozone Response to Emission Reductions in the Southeastern United States. *Atmos. Chem. Phys.* **2018**, *18* (11), 8183–8202.
- (35) Henneman, L. R. F.; Shen, H.; Liu, C.; Hu, Y.; Mulholland, J. A.; Russell, A. G. Responses in Ozone and Its Production Efficiency Attributable to Recent and Future Emissions Changes in the Eastern United States. *Environ. Sci. Technol.* **2017**, *51* (23), 13797–13805.
- (36) He, H.; Liang, X.-Z.; Sun, C.; Tao, Z.; Tong, D. Q. The Long-Term Trend and Production Sensitivity Change in the US Ozone Pollution from Observations and Model Simulations. *Atmos. Chem. Phys.* **2020**, *20* (5), 3191–3208.
- (37) Pusede, S. E.; Gentner, D. R.; Wooldridge, P. J.; Browne, E. C.; Rollins, A. W.; Min, K. E.; Russell, A. R.; Thomas, J.; Zhang, L.; Brune, W. H.; et al. On the Temperature Dependence of Organic Reactivity, Nitrogen Oxides, Ozone Production, and the Impact of Emission Controls in San Joaquin Valley, California. *Atmos. Chem. Phys.* **2014**, *14* (7), 3373–3395.
- (38) Wolff, G. T.; Dunker, A. M.; Rao, S. T.; Porter, P. S.; Zurbenko, I. G. Ozone Air Quality over North America: Part I—A Review of Reported Trends. *J. Air Waste Manage. Assoc.* **2001**, *51* (2), 273–282.
- (39) McDonald, B. C.; de Gouw, J. A.; Gilman, J. B.; Jathar, S. H.; Akherati, A.; Cappa, C. D.; Jimenez, J. L.; Lee-Taylor, J.; Hayes, P. L.; et al. Volatile chemical products emerging as largest petrochemical source of urban organic emissions. *Science* **2018**, *359* (6377), 760–764.
- (40) Guenther, A. B.; Jiang, X.; Heald, C. L.; Sakulyanontvittaya, T.; Duhl, T.; Emmons, L. K.; Wang, X. The Model of Emissions of Gases and Aerosols from Nature Version 2.1 (MEGAN2.1): An Extended and Updated Framework for Modeling Biogenic Emissions. *Geosci. Model Dev.* **2012**, *5* (6), 1471–1492.
- (41) Vukovich, F. M. Regional-Scale Boundary Layer Ozone Variations in the Eastern United States and Their Association with Meteorological Variations. *Atmos. Environ.* **1995**, *29* (17), 2259–2273.
- (42) Pierce, T.; Hogrefe, C.; Trivikrama Rao, S.; Porter, P. S.; Ku, J.-Y. Dynamic Evaluation of a Regional Air Quality Model: Assessing the Emissions-Induced Weekly Ozone Cycle. *Atmos. Environ.* **2010**, *44* (29), 3583–3596.
- (43) Boersma, F.; Eskes, H.; Richter, A.; Smedt, I. D.; Lorente, A.; Beirle, S.; van Geffen, J.; Peters, E.; Roozendael, M. V.; Wagner, T. QA4ECV NO<sub>2</sub> Tropospheric and Stratospheric Column Data from OMI, Royal Netherlands Meteorological Institute (KNMI), 2017, DOI: 10.21944/qa4ecv-no2-omi-v1.1.
- (44) Smedt, I. D.; Yu, H.; Richter, A.; Beirle, S.; Eskes, H.; Boersma, F.; Roozendael, M. V.; van Geffen, J.; Lorente, A.; Peters, E. QA4ECV HCHO Tropospheric Column Data from OMI, 2017 DOI: 10.18758/71021031.
- (45) Boersma, F.; Eskes, H.; Richter, A.; Smedt, I. D.; Lorente, A.; Beirle, S.; van Geffen, J.; Peters, E.; Roozendael, M. V.; Wagner, T. QA4ECV NO<sub>2</sub> Tropospheric and Stratospheric Column Data from GOME, 2017, DOI: 10.21944/qa4ecv-no2-gome-v1.1.
- (46) Boersma, F.; Eskes, H.; Richter, A.; Smedt, I. D.; Lorente, A.; Beirle, S.; van Geffen, J.; Peters, E.; Roozendael, M. V.; Wagner, T. QA4ECV NO<sub>2</sub> Tropospheric and Stratospheric Column Data from SCIAMACHY, 2017, DOI: 10.21944/qa4ecv-no2-scia-v1.1.
- (47) Lorente, A.; Folkert Boersma, K.; Yu, H.; Dorner, S.; Hilboll, A.; Richter, A.; Liu, M.; Lamsal, L. N.; Barkley, M.; De Smedt, I.; et al. Structural Uncertainty in Air Mass Factor Calculation for NO<sub>2</sub> and HCHO Satellite Retrievals. *Atmos. Meas. Tech.* **2017**, *10* (3), 759–782.
- (48) De Smedt, I.; Theys, N.; Yu, H.; Danckaert, T.; Lerot, C.; Compornolle, S.; Van Roozendael, M.; Richter, A.; Hilboll, A.; Peters, E.; et al. Algorithm Theoretical Baseline for Formaldehyde Retrievals from SSP TROPOMI and from the QA4ECV Project. *Atmos. Meas. Tech.* **2018**, *11* (4), 2395–2426.
- (49) Zara, M.; Boersma, K. F.; De Smedt, I.; Richter, A.; Peters, E.; van Geffen, J. H. G. M.; Beirle, S.; Wagner, T.; Van Roozendael, M.; Marchenko, S.; Lamsal, L. N.; Eskes, H. J. Improved Slant Column Density Retrieval of Nitrogen Dioxide and Formaldehyde for OMI and GOME-2A from QA4ECV: Intercomparison, Uncertainty Characterisation, and Trends. *Atmos. Meas. Tech.* **2018**, *11* (7), 4033–4058.
- (50) Williams, J. E.; Boersma, K. F.; Le Sager, P.; Verstraeten, W. W. The High-Resolution Version of TMS-MP for Optimized Satellite

Retrievals: Description and Validation. *Geosci. Model Dev.* **2017**, *10* (2), 721–750.

(51) Background information about the Row Anomaly in OMI <http://projects.knmi.nl/omi/research/product/rowanomaly-background.php>.

(52) Geddes, J. A.; Martin, R. V.; Boys, B. L.; van Donkelaar, A. Long-Term Trends Worldwide in Ambient NO<sub>2</sub> Concentrations Inferred from Satellite Observations. *Environ. Health Perspect.* **2016**, *124* (3), 281–289.

(53) Palmer, P. I.; Abbot, D. S.; Fu, T.-M.; Jacob, D. J.; Chance, K.; Kurosu, T. P.; Guenther, A.; Wiedinmyer, C.; Stanton, J. C.; Pilling, M. J.; Pressley, S. N.; Lamb, B.; Sumner, A. L. Quantifying the Seasonal and Interannual Variability of North American Isoprene Emissions Using Satellite Observations of the Formaldehyde Column. *J. Geophys. Res.* **2006**, *111* (D12), D12315.

(54) Zhu, L.; Jacob, D. J.; Keutsch, F. N.; Mickley, L. J.; Scheffe, R.; Strum, M.; Gonzalez Abad, G.; Chance, K.; Yang, K.; Rappengluck, B.; et al. Formaldehyde (HCHO) As a Hazardous Air Pollutant: Mapping Surface Air Concentrations from Satellite and Inferring Cancer Risks in the United States. *Environ. Sci. Technol.* **2017**, *51* (10), 5650–5657.

(55) Duncan, B. N.; Yoshida, Y.; Damon, M. R.; Douglass, A. R.; Witte, J. C. Temperature Dependence of Factors Controlling Isoprene Emissions. *Geophys. Res. Lett.* **2009**, *36* (5), 1886–5.

(56) Pusede, S. E.; Cohen, R. C. On the Observed Response of Ozone to NO<sub>x</sub> and VOC Reactivity Reductions in San Joaquin Valley California 1995–Present. *Atmos. Chem. Phys.* **2012**, *12* (18), 8323–8339.

(57) Pusede, S. E.; Steiner, A. L.; Cohen, R. C. Temperature and Recent Trends in the Chemistry of Continental Surface Ozone. *Chem. Rev.* **2015**, *115* (10), 3898–3918.

(58) de Foy, B.; Lu, Z.; Streets, D. G. Impacts of Control Strategies, the Great Recession and Weekday Variations on NO<sub>2</sub> Columns above North American Cities. *Atmos. Environ.* **2016**, *138* (C), 74–86.

(59) Kim, S. W.; Heckel, A.; McKeen, S. A.; Frost, G. J.; Hsie, E. Y.; Trainer, M. K.; Richter, A.; Burrows, J. P.; Peckham, S. E.; Grell, G. A. Satellite-observed U.S. Power Plant NO<sub>x</sub> emission Reductions and Their Impact on Air Quality. *Geophys. Res. Lett.* **2006**, *33* (22), L22812–5.

(60) Frost, G. J.; McKeen, S. A.; Trainer, M.; Ryerson, T. B.; Neuman, J. A.; Roberts, J. M.; Swanson, A.; Holloway, J. S.; Sueper, D. T.; Fortin, T.; Parrish, D. D.; Fehsenfeld, F. C.; Flocke, F.; Peckham, S. E.; Grell, G. A.; Kowal, D.; Cartwright, J.; Auerbach, N.; Habermann, T. Effects of Changing Power Plant NO<sub>x</sub> emissions on Ozone in the Eastern United States: Proof of Concept. *J. Geophys. Res.* **2006**, *111* (D12), D12306–19.

(61) Russell, A. R.; Valin, L. C.; Cohen, R. C. Trends in OMI NO<sub>2</sub> Observations over the United States: Effects of Emission Control Technology and the Economic Recession. *Atmos. Chem. Phys.* **2012**, *12* (24), 12197–12209.

(62) Abbot, D. S.; Palmer, P. I.; Martin, R. V.; Chance, K. V.; Jacob, D. J.; Guenther, A. Seasonal and Interannual Variability of North American Isoprene Emissions as Determined by Formaldehyde Column Measurements from Space. *Geophys. Res. Lett.* **2003**, *30* (17), 1886.

(63) Chen, W. H.; Guenther, A. B.; Wang, X. M.; Chen, Y. H.; Gu, D. S.; Chang, M.; Zhou, S. Z.; Wu, L. L.; Zhang, Y. Q. Regional to Global Biogenic Isoprene Emission Responses to Changes in Vegetation From 2000 to 2015. *J. Geophys. Res.: Atmos.* **2018**, *123* (7), 3757–3771.

(64) Wolfe, G. M.; Kaiser, J.; Hanisco, T. F.; Keutsch, F. N.; de Gouw, J. A.; Gilman, J. B.; Graus, M.; Hatch, C. D.; Holloway, J.; Horowitz, L. W.; Lee, B. H.; Lerner, B. M.; Lopez-Hilafiker, F.; Mao, J.; Marvin, M. R.; Peischl, J.; Pollack, I. B.; Roberts, J. M.; Ryerson, T. B.; Thornton, J. A.; Veres, P. R.; Warneke, C. Formaldehyde Production from Isoprene Oxidation across NO<sub>x</sub> Regimes. *Atmos. Chem. Phys.* **2016**, *16* (4), 2597–2610.

(65) Sourì, A. H.; Nowlan, C. R.; Wolfe, G. M.; Lamsal, L. N.; Chan Miller, C. E.; Abad, G. G.; Janz, S. J.; Fried, A.; Blake, D. R.;

Weinheimer, A. J.; Diskin, G. S.; Liu, X.; Chance, K. Revisiting the Effectiveness of HCHO/NO<sub>2</sub> Ratios for Inferring Ozone Sensitivity to Its Precursors Using High Resolution Airborne Remote Sensing Observations in a High Ozone Episode during the KORUS-AQ Campaign. *Atmos. Environ.* **2020**, *224*, 117341.

(66) Zhu, L.; Mickley, L. J.; Jacob, D. J.; Marais, E. A.; Sheng, J.; Hu, L.; Abad, G. G.; Chance, K. Long-Term (2005–2014) Trends in Formaldehyde (HCHO) Columns across North America as Seen by the OMI Satellite Instrument: Evidence of Changing Emissions of Volatile Organic Compounds. *Geophys. Res. Lett.* **2017**, *44* (13), 7079–7086.

(67) Spinei, E.; Whitehill, A.; Fried, A.; Tiefengraber, M.; Knepp, T. N.; Herndon, S.; Herman, J. R.; Müller, M.; Abuhassan, N.; Cede, A.; Richter, D.; Walega, J.; Crawford, J.; Szykman, J.; Valin, L.; Williams, D. J.; Long, R.; Swap, R. J.; Lee, Y.; Nowak, N.; Poche, B. The First Evaluation of Formaldehyde Column Observations by Improved Pandora Spectrometers during the KORUS-AQ Field Study. *Atmos. Meas. Tech.* **2018**, *11* (9), 4943–4961.

(68) Li, J.; Wang, Y.; Qu, H. Dependence of Summertime Surface Ozone on NO and VOC Emissions Over the United States: Peak Time and Value. *Geophys. Res. Lett.* **2019**, *46* (6), 3540–3550.

(69) Lindsay, R. W.; Richardson, J. L.; Chameides, W. L. Ozone Trends in Atlanta, Georgia: Have Emission Controls Been Effective? *JAPCA* **1989**, *39* (1), 40–43.

(70) Chameides, W.; Lindsay, R.; Richardson, J.; Kiang, C. The Role of Biogenic Hydrocarbons in Urban Photochemical Smog: Atlanta as a Case Study. *Science* **1988**, *241* (4872), 1473.

(71) Parrish, D. D.; Singh, H. B.; Molina, L.; Madronich, S. Air Quality Progress in North American Megacities: A Review. *Atmos. Environ.* **2011**, *45* (39), 7015–7025.

(72) Lin, M.; Horowitz, L. W.; Payton, R.; Fiore, A. M.; Tonnesen, G. US Surface Ozone Trends and Extremes from 1980 to 2014: Quantifying the Roles of Rising Asian Emissions, Domestic Controls, Wildfires, and Climate. *Atmos. Chem. Phys.* **2017**, *17* (4), 2943–2970.

(73) Pollack, I. B.; Ryerson, T. B.; Trainer, M.; Neuman, J. A.; Roberts, J. M.; Parrish, D. D. Trends in Ozone, Its Precursors, and Related Secondary Oxidation Products in Los Angeles, California: A Synthesis of Measurements from 1960 to 2010. *Journal of Geophysical Research: Atmospheres* **2013**, *118* (11), 5893–5911.

(74) Murphy, J. G.; Day, D. A.; Cleary, P. A.; Wooldridge, P. J.; Millet, D. B.; Goldstein, A. H.; Cohen, R. C. The Weekend Effect within and Downwind of Sacramento - Part 1: Observations of Ozone, Nitrogen Oxides, and VOC Reactivity. *Atmos. Chem. Phys.* **2007**, *7* (20), 5327–5339.

(75) Marr, L. C.; Harley, R. A. Modeling the Effect of Weekday-Weekend Differences in Motor Vehicle Emissions on Photochemical Air Pollution in Central California. *Environ. Sci. Technol.* **2002**, *36* (19), 4099–4106.

(76) Baidar, S.; Hardesty, R. M.; Kim, S. W.; Langford, A. O.; Oetjen, H.; Senff, C. J.; Trainer, M.; Volkamer, R. Weakening of the Weekend Ozone Effect over California's South Coast Air Basin. *Geophys. Res. Lett.* **2015**, *42* (21), 9457–9464.

(77) Wolff, G. T.; Kahlbaum, D. F.; Heuss, J. M. The Vanishing Ozone Weekday/Weekend Effect. *J. Air Waste Manage. Assoc.* **2013**, *63* (3), 292–299.

(78) Forster, P.; Solomon, S. Observations of a “Weekend Effect” in Diurnal Temperature Range. *Proc. Natl. Acad. Sci. U. S. A.* **2003**, *100* (20), 11225–11230.

(79) Sillman, S.; He, D. Some Theoretical Results Concerning O<sub>3</sub>-NO<sub>x</sub>-VOC Chemistry and NO<sub>x</sub>-VOC Indicators. *J. Geophys. Res.* **2002**, *107* (D22), 4659–15.

(80) Chan Miller, C.; Jacob, D. J.; Marais, E. A.; Yu, K.; Travis, K. R.; Kim, P. S.; Fisher, J. A.; Zhu, L.; Wolfe, G. M.; Hanisco, T. F.; et al. Glyoxal Yield from Isoprene Oxidation and Relation to Formaldehyde: Chemical Mechanism, Constraints from SENEX Aircraft Observations, and Interpretation of OMI Satellite Data. *Atmos. Chem. Phys.* **2017**, *17* (7), 8725.

(81) Chen, X.; Millet, D. B.; Singh, H. B.; Wisthaler, A.; Apel, E. C.; Atlas, E. L.; Blake, D. R.; Bourgeois, I.; Brown, S. S.; Crounse, J. D.;

et al. On the Sources and Sinks of Atmospheric VOCs: An Integrated Analysis of Recent Aircraft Campaigns over North America. *Atmos. Chem. Phys.* **2019**, *19* (14), 9097–9123.

(82) Veefkind, J. P.; Aben, I.; McMullan, K.; Förster, H.; de Vries, J.; Otter, G.; Claas, J.; Eskes, H. J.; de Haan, J. F.; Kleipool, Q.; van Weele, M.; Hasekamp, O.; Hoogeveen, R.; Landgraf, J.; Snel, R.; Tol, P.; Ingmann, P.; Voors, R.; Kruizinga, B.; Vink, R.; Visser, H.; Levelt, P. F. TROPOMI on the ESA Sentinel-5 Precursor: A GMES Mission for Global Observations of the Atmospheric Composition for Climate, Air Quality and Ozone Layer Applications. *Remote Sensing of Environment* **2012**, *120* (C), 70–83.

(83) Zoogman, P.; Liu, X.; Suleiman, R. M.; Pennington, W. F.; Flittner, D. E.; Al-Saadi, J. A.; Hilton, B. B.; Nicks, D. K.; Newchurch, M. J.; Carr, J. L.; et al. Tropospheric Emissions: Monitoring of Pollution (TEMPO). *J. Quant. Spectrosc. Radiat. Transfer* **2017**, *186*, 17–39.